Research Article

Mathematical Methods in the Applied Sciences

Received 18 May 2011

Published online 24 May 2012 in Wiley Online Library

(wileyonlinelibrary.com) DOI: 10.1002/mma.2582
MOS subject classification: 35R25; 35B60; 35K10; 65M20; 65M30

Reconstructing the past from imprecise knowledge of the present: Effective non-uniqueness in solving parabolic equations backward in time

Alfred S. Carasso[*†]

Communicated by P. Sacks

Identifying sources of ground water pollution and deblurring astronomical galaxy images are two important applications generating growing interest in the numerical computation of parabolic equations backward in time. However, while backward uniqueness typically prevails in parabolic equations, the precise data needed for the existence of a particular backward solution is seldom available. This paper discusses previously unexplored non-uniqueness issues, originating from trying to reconstruct a particular solution from imprecise data. Explicit 1D examples of linear and nonlinear parabolic equations are presented, in which there is strong computational evidence for the *existence* of distinct solutions $w^{\mathbf{red}}(x,t)$ and $w^{\mathbf{green}}(x,t)$, on $0 \le t \le 1$. These solutions have the property that the traces $w^{\mathbf{red}}(x,1)$ and $w^{\mathbf{green}}(x,1)$ at time $t = 1$ are close enough to be visually indistinguishable, while the corresponding initial values $w^{\mathbf{red}}(x,0)$ and $w^{\mathbf{green}}(x,0)$ are vastly different, well-behaved, physically plausible functions, with comparable L^2 norms. This implies effective non-uniqueness in the recovery of $w^{\mathbf{red}}(x,0)$ from approximate data for $w^{\mathbf{red}}(x,1)$. In all these examples, the Van Cittert iterative procedure is used as a tool to discover unsuspected, valid, additional solutions $w^{\mathbf{green}}(x,0)$. This methodology can generate numerous other examples and indicates that multidimensional problems are likely to be a rich source of striking non-uniqueness phenomena. Published 2012. This article is a US Government work and is in the public domain in the USA.

Keywords: advection dispersion equation; backward parabolic equations; hydrologic inversion; image deblurring; ill-posed continuation; non-uniqueness; Van Cittert iteration.

1. Introduction

Uniqueness backward in time is a characteristic feature of a large class of parabolic equations. In practice however, at a given positive time, the precise data needed for the existence of a particular backward solution are seldom available, and one must use approximate values. This paper discusses computationally generated 1D examples of effective non-uniqueness, originating from trying to reconstruct a particular solution from imprecise data. These examples are unexpected and of a type not previously known in the literature, to the author's knowledge. Such non-uniqueness is of major significance in applications. Resolving the increased uncertainty in backward reconstructions may require more detailed prior information about the true solution than is available. The methodology used to create these examples can generate numerous other examples. Multidimensional problems are likely to be a rich source of striking non-uniqueness phenomena.

As is well known, backward parabolic equations are notoriously ill-posed and prone to amplification of high-frequency noise in the input data. Such instability can create the appearance of non-uniqueness. As shown in [1] for the case of the 1D heat equation on a finite interval, perturbing the input data at time $t = 1$ by adding a spurious high-frequency sinusoid, with almost imperceptible amplitude, can result in a noticeably different solution at $t = 0$, where that amplified sinusoid becomes highly visible. To prevent such spurious oscillations, smoothness constraints, together with non-negativity constraints when required by physics, have long been used in backward parabolic problems to regularize the inversion. Indeed, smoothness and non-negativity constraints are widely used in many other ill-posed contexts.

Applied and Computational Mathematics Division, National Institute of Standards and Technology, Gaithersburg, MD 20899, USA
**Correspondence to: Alfred S. Carasso, Applied and Computational Mathematics Division, National Institute of Standards and Technology, Gaithersburg, MD 20899, USA.*
†E-mail: alfred.carasso@nist.gov

However, the non-uniqueness phenomena discussed here do not exhibit obvious tell-tale features and cannot be prevented by imposing smoothness and non-negativity constraints. Linear and nonlinear examples are given with 'false' solutions that are qualitatively quite similar to the true solution. Examples are also given with smooth, non-negative true solutions, yet with 'false' solutions that are also non-negative, smoother, and perhaps even more plausible. Moreover, such effective non-uniqueness can occur even with fairly accurate approximate data at time $t = 1$.

There has been growing interest in recent years in the development of numerical methods for solving parabolic equations backward in time. In [1–15], various useful methods are analyzed and illustrated with interesting test computations. Currently, the two most significant areas of application of backward parabolic equations are *hydrologic inversion* and *image deblurring*. In hydrologic inversion, the aim is to identify sources of groundwater pollution by reconstructing the contaminant plume history. This involves solving the advection dispersion equation backward in time, given the contaminant spatial distribution $g(x, y)$ at the current time T,

$$\begin{aligned} C_t &= \nabla.\{D\nabla C\} - \nabla.\{v\, C\}, \quad 0 < t \le T, \\ C(x, y, T) &= g(x, y), \quad (x, y) \in R^2. \end{aligned} \tag{1}$$

Here, C is the mass concentration, D is the diffusion tensor, and v is the velocity vector. There is a large literature on this topic. Instructive expository discussions of this problem, together with backward calculations of realistic examples, principally in 1D, may be found in [16–23].

Brownian motion is pervasive in many branches of science, including image science. For this reason, images blurred by Gaussian point spread functions are a common occurrence. Deblurring Gaussian blur is mathematically equivalent to solving the heat conduction equation backward in time, with the noisy blurred image $g(x, y)$ as data at time $t = 1$ and with conduction coefficient $\alpha > 0$ proportional to the point spread variance,

$$\begin{aligned} w_t &= \alpha \Delta w, \quad 0 < t \le 1, \\ w(x, y, 1) &= g(x, y), \quad (x, y) \in R^2. \end{aligned} \tag{2}$$

A discussion of this problem may be found in [24–29]. In many areas of applied science, the underlying random process involves a fundamental modification of Brownian motion, whereby the motion takes place in a specific randomized operational time $Q(t)$, rather than in standard clock time t. This new *subordinated* Brownian process leads to non-standard diffusion equations. Such notions have also been found useful in image deblurring. In [30], and references therein, backward in time problems for 2D fractional and/or logarithmic diffusion equations,

$$w_t = -\alpha(-\Delta)^{\beta} w, \quad w_t = -\left[\lambda \log\left\{1 + \gamma(-\Delta)^{\beta}\right\}\right] w, \quad 0 < t \le 1, \tag{3}$$

are successfully applied, in a blind deconvolution scheme, to enhance Hubble Space Telescope images, as well as scanning electron microscope images of interest in nanotechnology. In (3), α, β, λ, and γ are positive constants, with $\beta < 1$.

2. Stabilized problems, backward uniqueness, and stability estimates

Theoretical discussions of backward parabolic equations and other non-standard problems may be found in [31–35] and the references therein. Backward parabolic equations are classical examples of ill-posed problems in the sense of Hadamard. Typically, a backward solution exists only for highly restricted data satisfying certain smoothness and other requirements that are not easily characterized. In most cases of practical interest, when a solution exists, it is unique. However, backward solutions depend discontinuously on the data for which they exist and slight changes in that data can result in very large, if not explosive, changes in the corresponding solutions.

Backward parabolic equations can be stabilized by prescribing an *a-priori* bound M for the L^2 norm of the solution at time $t = 0$. The following situation illustrates the general ideas. Let Ω be a bounded domain in R^n with smooth boundary $\partial\Omega$. Let L be an elliptic operator in Ω acting on smoothly differentiable functions vanishing on $\partial\Omega$. In the simplest case, L is a linear self-adjoint differential operator with variable coefficients that may depend on time. However, we will also consider nonlinear problems. In all cases, the forward equation $w_t = Lw, t > 0$, is well-posed. The stabilized backward parabolic problem for L may be stated as follows. Given $f(x) \in L^2(\Omega)$ and $M, \delta > 0$, with $\delta \ll M$, find all solutions of

$$w_t = Lw, \;\; x \in \Omega, \qquad w = 0, \; x \in \partial\Omega, \quad 0 < t \le T, \tag{4}$$

such that

$$\| w(.,T) - f \|_2 \le \delta, \quad \| w(.,0) \|_2 \le M. \tag{5}$$

It is assumed that $f(x), \delta$, and M are compatible with the existence of solutions. Here, $f(x)$ is presumed to be a sufficiently close L^2 approximation to the exact values $w(x, T)$ at $t = T$, of a solution $w(x, t)$ of (4), believed to satisfy $\| w(.,0) \|_2 \le M$. In many engineering or applied science contexts, only educated guesses would generally be available to estimate δ and M, rather than exact values. Typically, the L^2 relative error

$$\| w(.,T) - f \|_2 \,/\, \| w(.,T) \|_2 \le \delta / \{\| f \|_2 - \delta\} \approx \delta / \| f \|_2, \tag{6}$$

might be expected to be on the order of 1% or thereabouts. Since the given data $f(x)$ may simultaneously approximate several distinct solutions $w^p(x, t)$ of (4) at time T, there are, in general, infinitely many possible solutions of (4) and (5). If δ is small, it is generally assumed

that any two such solutions would differ only slightly. The extent to which this expectation is justified is determined by the backward stability inequality governing the particular parabolic equation $w_t = Lw$.

The following *logarithmic convexity* method [31, 33, 35] is often used to obtain stability inequalities for ill-posed continuation problems. Let $w^1(x,t)$ and $w^2(x,t)$ be any two solutions of the equation $w_t = Lw$. For $0 \le t \le T$, let $F(t) = \| w^1(.,t) - w^2(.,t) \|_2^2$. With the use of the properties of the differential operator L, together with appropriate restrictions on the class of solutions being considered, the aim is to establish the following inequality

$$F(t)F''(t) - \{F'(t)\}^2 \ge -a_1 F(t)F'(t) - a_2 F^2(t), \quad 0 < t < T, \tag{7}$$

where a_1 and a_2 are constants.

If $a_1 = a_2 = 0$ in (7), then $\log F(t)$ is a convex function of t and

$$F(t) \le \{F(0)\}^{(T-t)/T} \{F(T)\}^{t/T}, \quad 0 \le t \le T. \tag{8}$$

More typically, $a_1 \ne 0$ in (7). In that case, let

$$q = -a_2/2a_1, \quad \mu(t) = \left\{e^{-a_1 t} - 1\right\} \left\{e^{-a_1 T} - 1\right\}^{-1}, \quad 0 \le t \le T. \tag{9}$$

Then, as shown in [31, 33, 35],

$$e^{2qt} F(t) \le \{F(0)\}^{1-\mu(t)} \left\{e^{2qT} F(T)\right\}^{\mu(t)}, \quad 0 \le t \le T. \tag{10}$$

Inequalities of this type have been obtained for a wide class of problems, in addition to the class of parabolic equations $w_t = Lw$ considered in this paper; see [31–35]. For solutions satisfying a prescribed L^2 bound M at $t = 0$, we obtain from (10), for $0 \le t \le T$,

$$e^{qt} \| w^1(.,t) - w^2(.,t) \|_2 \le \{2M\}^{1-\mu(t)} \left\{e^{qT} \| w^1(.,T) - w^2(.,T) \|_2\right\}^{\mu(t)}. \tag{11}$$

This inequality establishes L^2 Hölder-continuous dependence of solutions at any fixed t with $0 < t \le T$, on the data at time T. The Hölder exponent $\mu(t)$ satisfies $0 \le \mu(t) \le 1$, with $\mu(t) > 0, t > 0, \mu(T) = 1, \mu(0) = 0$, and $\mu(t) \downarrow 0$ monotonically as $t \downarrow 0$.

2.1. *Backward uniqueness*

The inequality (11) implies backward uniqueness of solutions satisfying a prescribed bound. Indeed, if $\| w^1(.,T) - w^2(.,T) \|_2 = 0$, then $\| w^1(.,t) - w^2(.,t) \|_2 = 0$ for every $0 < t \le T$, since $\mu(t) > 0$ for $t > 0$. By continuity, $\| w^1(.,t) - w^2(.,t) \|_2 = 0$ on $0 \le t \le T$.

Remarkably, backward uniqueness even holds true for the Navier–Stokes equations. This landmark result was obtained in [34] by establishing the stability inequality (10) appropriate for these equations.

2.2. *Backward continuity*

We may now address the recoverability of solutions in the stabilized backward problem (4), (5). Let $w^1(x,t), w^2(x,t)$ be any two possible solutions of (4), (5). Then,

$$\| w^1(.,0) - w^2(.,0) \|_2 \le 2M, \quad \| w^1(.,T) - w^2(.,T) \|_2 \le 2\delta. \tag{12}$$

Hence, from (11),

$$e^{qt} \| w^1(.,t) - w^2(.,t) \|_2 \le 2M^{1-\mu(t)} \left\{e^{qT}\delta\right\}^{\mu(t)}, \quad 0 \le t \le T. \tag{13}$$

Here, the dependence of the Hölder exponent $\mu(t)$ on t, illustrated in Figure 1, plays a crucial role. In the best possible case, that of a linear self-adjoint elliptic operator L with time-independent coefficients, we have $\mu(t) = t/T$, so that $\mu(t)$ decays linearly to zero as continuation progresses from $t = T$ to $t = 0$. At $t = T/2$, we have $\mu(T/2) = 1/2$ and with the assumption that $q = 0$, $\| w^1(.,T/2) - w^2(.,T/2) \|_2 \le 2\sqrt{M\delta}$. This loss of acccuracy from $O(\delta)$ to $O\left(\sqrt{\delta}\right)$, while still only half way to $t = 0$, is noteworthy. More typically, with $a_1 < 0$ in (7), $\mu(t)$ is *sublinear* in t, possibly with rapid exponential decay. This can lead to much more severe loss of accuracy as reconstruction progresses to $t = 0$. As shown in [32], rapid decay of μ to zero can be brought about by various factors, including nonlinearity, non-self-adjointness, diffusion coefficients that grow rapidly with time, or adverse spectral properties in the elliptic operator L. In all cases, (13) does not guarantee any accuracy at $t = 0$, but only provides the redundant information $\| w^1(.,0) - w^2(.,0) \|_2 \le 2M$.

While inequality (13) is best possible in general, it necessarily contemplates worst case scenarios that may be too pessimistic in some applications. Indeed, successful recoveries of contaminant plumes in hydrology, as well as striking enhancement of Hubble telescope galaxy images, have been documented [18, 19, 30]. Nevertheless, the behavior of the Hölder exponents in (13) reflects a basic underlying truth. This behavior is indicative of the rate at which the particular evolution equation $w_t = Lw$ has forgotten the past and, hence, of the subsequent difficulty of reconstructing the past from imperfect knowledge of the present. This paper illuminates this deeper meaning by exhibiting specific 1D parabolic equations on $0 \le t \le 1$, with distinct solutions $w^{\text{red}}(x,t)$ and $w^{\text{green}}(x,t)$. These solutions are such that their traces at $t = 1$, $w^{\text{red}}(x,1), w^{\text{green}}(x,1)$, approximate one another with an L^2 relative error typically smaller than 1% and are visually indistinguishable. However, their corresponding initial values $w^{\text{red}}(x,0), w^{\text{green}}(x,0)$, are vastly different. Therein lies the difficulty of reconstructing the correct backward solution from approximate data at $t = 1$.

Published 2012. This article is a US Government work and is in the public domain in the USA.

Math. Meth. Appl. Sci. **2013**, 36 249–261

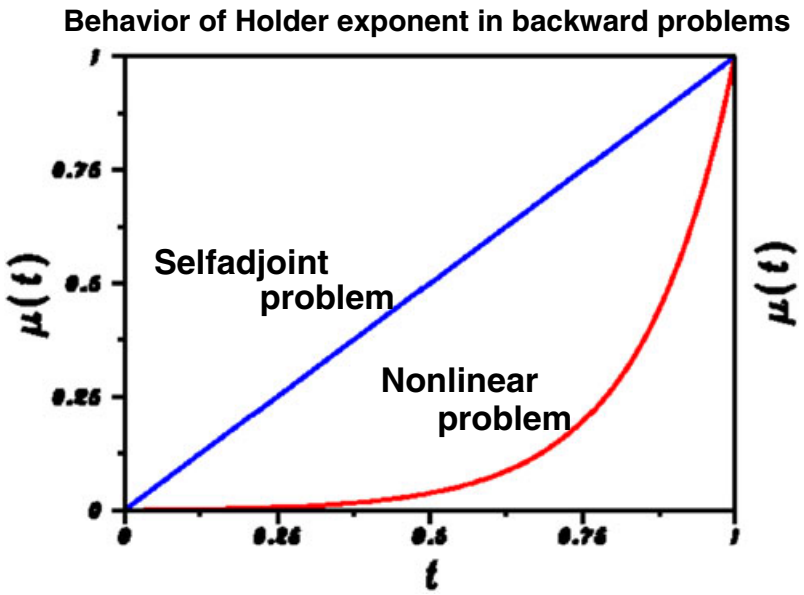

Figure 1. Behavior of Hölder exponent $\mu(t)$ in inequality (13) reflects rate at which the forward evolution equation $w_t = Lw$ has forgotten the past, as t increases from $t = 0$ to $t = T = 1$. Deviations away from a linear, time-independent, self-adjoint spatial differential operator L can lead to exponential decay in $\mu(t), t \downarrow 0$, and affect backward reconstruction from $t = T$.

3. Exploring backward solutions using Van Cittert iterations

Consider the well-posed, forward, linear, or nonlinear parabolic initial value problem $w_t = Lw, 0 < t \leq 1, w(x,0) = w_0^{\text{red}}(x)$. Define S to be the associated solution operator at time $t = 1$. Thus, given any $h(x)$ in $L^2(\Omega)$, the operator S uses $h(x)$ as initial data $w(x,0)$ in (4) and produces the corresponding solution $w_h(x,1)$ at $t = 1$, so that $S[h(x)] = w_h(x,1)$. In particular, $S\left[w_0^{\text{red}}(x)\right] = w^{\text{red}}(x,1)$. Next, let $f(x)$ be an approximation to $w^{\text{red}}(x,1)$ with $\| w^{\text{red}}(.,1) - f \|_2 \leq \delta$, as in (5). With fixed relaxation parameter $\gamma > 0$, and with $h^1(x) = \gamma f(x)$, consider the following iterative procedure

$$h^{n+1}(x) = h^n(x) + \gamma \left\{ f(x) - S\left[h^n(x)\right] \right\}, \quad n \geq 1. \tag{14}$$

In spectroscopy and image processing, with S an explicitly known linear convolution integral operator, this procedure is the widely used Van Cittert iteration [36, 37]. In these applications, the Van Cittert method generally produces useful results after finitely many iterations although it may not converge. In the present case, S may be highly nonlinear and is not known explicitly. For given $h(x)$ in $L^2(\Omega)$, $S[h(x)]$ must be obtained by numerically solving the well-posed forward parabolic problem.

Clearly, in the present parabolic context, the Van Cittert iteration is unlikely to converge. Indeed, if $h^n \to h^\dagger$ in $L^2(\Omega)$ in (14), then $S[h^\dagger(x)] = f(x)$. However, $S[h^\dagger(x)]$ necessarily satisfies highly restrictive smoothness requirements, and these are not likely to be met by the given approximate data $f(x)$. Nevertheless, as will be seen below, the Van Cittert iteration is a valuable exploratory tool. In a wide variety of 1D linear and nonlinear parabolic equations, this procedure typically generates iterates $h^n(x)$ such that the L^∞ norm of the residual, $\| f - S[h^n] \|_\infty$, decays quasi monotonically to a small value after finitely many iterations. This is often sufficient for our purpose. From (5), if for some positive integer N we find $\| f - S[h^N] \|_2 \leq \delta$, with $\| h^N \|_2 \leq M$, then $h^N(x)$ is a valid candidate reconstruction of $w^{\text{red}}(x,0)$, given the approximation $f(x)$ to the unavailable $w^{\text{red}}(x,1)$. In the first four examples below, we have $\delta \leq$ 8.0E-3, $\delta/M \leq$ 2.0E-3. The last example has $\delta =$3.7E-2, $\delta/M =$1.2E-2.

An unexpected dividend of the truncated Van Cittert iteration is its ability to produce reconstructions that are relatively noise free. This 'self-regularizing' property is commonly observed in several iterative image restoration procedures, [25, 37].

4. Numerical implementation of Van Cittert's iteration

All of the examples discussed below are one dimensional, take place on the interval $-1 \leq x \leq 1$, involve smooth coefficients and initial values, and have homogeneous Dirichlet boundary conditions. To implement the iterative process in (14), use is made of an efficient, highly accurate parabolic equation solver. This method of lines procedure is discussed in [38] and is implemented as subroutine *D03PDF/D03PDA* in the NAG Mathematical Software Library. It uses Chebyshev C^0 collocation for spatial differencing, together with backward time differencing to advance the solution forward in time. Here, one hundred equispaced breakpoints, $-1 = x_1 < x_2 < x_3 < \cdots < x_{100} = 1$, are placed on $[-1, 1]$. Between each pair of breakpoints, the solution of $w_t = Lw$ is approximated by a cubic Chebyshev polynomial whose space and time derivatives are made to satisfy the parabolic equation at two collocation points chosen internally by the subroutine. C^0 continuity is enforced at the breakpoints. This leads to a total of 298 (non equispaced) mesh points on $[-1, 1]$. For each $t_k = k\Delta t$, the computed solution $w(x, t_k)$ is a piecewise cubic polynomial in x on $[-1, 1]$.

Published 2012. This article is a US Government work and is in the public domain in the USA.

All five examples below will follow the same road map. With initial data $w_0^{\text{red}}(x)$, the parabolic problem $w_t = Lw$ is first integrated up to time $t = 1$, to produce a presumed good approximation $f(x)$ to the unknown true solution $w^{\text{red}}(x, 1)$. This calculated $f(x)$, shown as a black curve in the figures, is then viewed as given data in an applied science or engineering context and is used in the Van Cittert procedure (14) to recover the unknown initial value $w_f(x, 0)$ that gave rise to $f(x)$ at $t = 1$. However, it will turn out that $f(x)$ is also a close approximation to an unsuspected additional solution $w^{\text{green}}(x, 1)$ corresponding to initial data $w_0^{\text{green}}(x)$ that can be vastly different from $w_0^{\text{red}}(x)$. A small perturbation of $f(x)$ can result in yet another candidate initial value, $w_0^{\text{blue}}(x)$, as shown in Example 5. The relaxation parameter γ in (14) was set to 0.5 in all five examples.

5. Example 1 (Figure 2). Linear self-adjoint

The following relatively well-behaved example is used to set the stage for the less well-behaved examples to follow. With $a = 0.05$, $\alpha = 0.05, \sigma = 0.025$, consider the linear, self-adjoint, variable coefficient problem

$$\begin{aligned} w_t &= a\left\{e^{(\sigma x+\alpha t)}w_x\right\}_x, \quad -1 < x < 1, \ \ 0 < t \le 1.0, \\ w(x,0) &= e^{2x}\sin(2\pi x), \quad -1 \le x \le 1, \quad w(-1,t) = w(1,t) = 0, \ \ t \ge 0. \end{aligned} \tag{15}$$

The initial value in (15), denoted by $w_0^{\text{red}}(x)$, is shown as the red trace in Figure 2. Using the parabolic solver in Section 4, the computed solution at time $t = 1$, denoted by $f(x)$, is shown as the black trace in Figure 2. While that computed solution is, in fact, an excellent approximation, we view $f(x)$ as merely a good approximation to the unknown true solution $w^{\text{red}}(x, 1)$ with $\| w^{\text{red}}(., 1) - f \|_2 \le \delta$. We stress that in an actual engineering application with real data, the expected L^2 relative error $\delta / \| f \|_2$ might be on the order of 1% or thereabouts. Using $f(x)$ in the Van Cittert procedure (14), we seek to recover the unknown initial values $w_f(x, 0)$ that gave rise to $f(x)$ at $t = 1$. For each successive iterate $h^n(x)$ in (14), we can evaluate and monitor the L^∞ residual, $\| f - S[h^n] \|_\infty$, as well as the L^2 relative error at $t = 1$, $\| f - S[h^n] \|_2 / \| f \|_2$. In this example, these two errors decay monotonically.

After 200 iterations, the L^∞ residual is 3.1E-3, so that the trace of $S[h^{200}](x)$ is visually indistinguishable from that of $f(x)$, while the L^2 relative error at $t = 1$ is 0.4%. The iterate $h^{200}(x)$ is shown as the green trace $w_0^{\text{green}}(x)$ in Figure 2. Moreover, $\| w_0^{\text{red}} \|_2 = 1.8$, while $\| w_0^{\text{green}} \|_2 = 1.7$. Therefore, both solutions $w^{\text{red}}(x, t)$ and $w^{\text{green}}(x, t)$ satisfy

$$\| w(., 1) - f \|_2 \le \delta \le 0.004 \| f \|_2, \qquad \| w(., 0) \|_2 \le M = 1.8. \tag{16}$$

Since $\| f \|_2 = 0.36$, we have $\delta \le 1.44\text{E-}3$, and $\delta/M \le 8\text{E-}4$. Thus, given only the approximate data $f(x)$, $w_0^{\text{green}}(x)$ in Figure 2 can be considered a valid reconstruction of the unknown initial data. Evidently, $f(x)$ is a close approximation to (at least) two distinct true solutions at $t = 1$, $w^{\text{red}}(x, 1)$ and $w^{\text{green}}(x, 1)$. These two solutions have visually indistinguishable traces at $t = 1$, but have distinct traces at $t = 0$. In this example, either reconstruction at $t = 0$ might be considered successful.

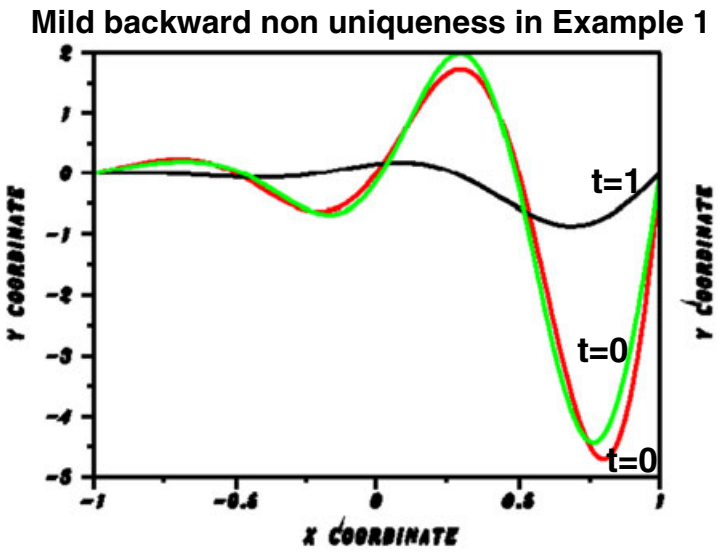

Figure 2. Well-behaved self-adjoint problem. Data $f(x)$ (black curve), approximating solution $w^{\text{red}}(x, t)$ at time $t = 1$ with an L^2 relative error of 0.41%, recovers reasonably close initial value $w_0^{\text{green}}(x)$, in lieu of true initial value $w_0^{\text{red}}(x)$.

6. Example 2 (Figure 3). Burgers equation

Behavior in this instructive nonlinear example involving Burgers equation is strikingly different from that in Example 1, although very similar solutions are involved. With $a = 0.05$, consider

$$\begin{aligned} w_t &= a(w_x)_x - ww_x, \ -1 < x < 1, \ 0 < t \le 1.0, \\ w(x,0) &= e^{2x}\sin(2\pi x), \quad -1 \le x \le 1, \ w(-1,t) = w(1,t) = 0, \ t \ge 0. \end{aligned} \tag{17}$$

The initial value $w_0^{\text{red}}(x)$ in (17) is shown as the red trace in Figure 3 (bottom), while the computed approximation $f(x)$ to $w^{\text{red}}(x,1)$ is shown as the black trace in the same figure. The red and black traces in Figure 3 (bottom) bear much the same qualitative and quantitative relationships to each other that characterize the corresponding traces in Figure 2. By using $f(x)$ in (14), the Van Cittert procedure was applied for 40 000 iterations, resulting in a final L^∞ residual of 7.8E-6, and an L^2 relative error at $t = 1$ of 0.00122%. That relative error is 300 times smaller than was the case in Example 1. The behavior of $\log\{\| f - S[h^n] \|_\infty\}$ versus n, is shown in Figure 3

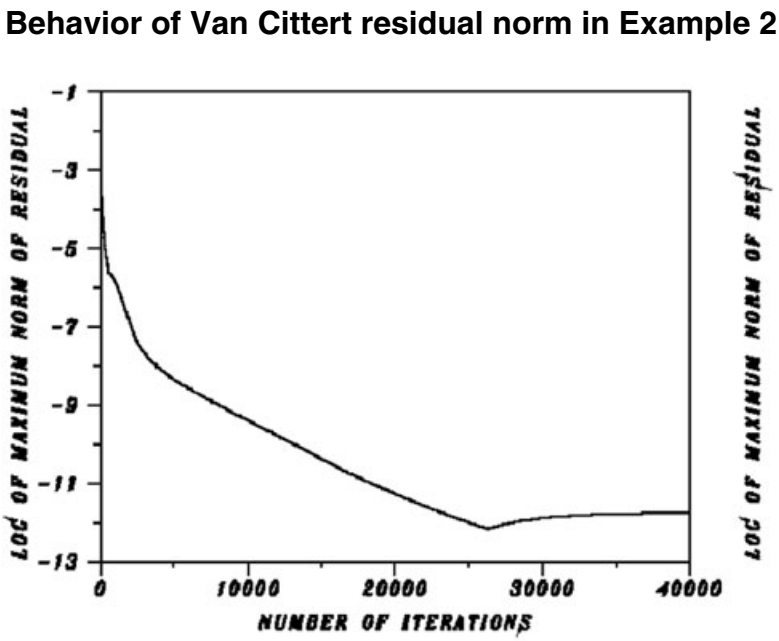

Figure 3. TOP. Behavior of $log\{\| f - S[h^n] \|_\infty\}$ for first 40 000 iterations n, in Van Cittert procedure in Example 2. BOTTOM. Intractable recovery in nonlinear Burgers equation. Despite highly accurate data $f(x)$ (black curve) approximating solution $w^{\text{red}}(x,t)$ at time $t = 1$ with an L^2 relative error of 0.00122%, true initial value $w_0^{\text{red}}(x)$ is not recovered. Valid, but noticeably different initial value $w_0^{\text{green}}(x)$ is obtained. Compare with self-adjoint behavior in Figure 2.

(top). Clearly, $S[h^{40\,000}(x)]) = w^{\text{green}}(x,1)$ is a very accurate match to the given data $f(x)$ and to $w^{\text{red}}(x,1)$. However, even with such small residuals, $h^{40\,000}(x) = w_0^{\text{green}}(x)$, shown as the green trace in Figure 3 (bottom), differs markedly from $w_0^{\text{red}}(x)$. The two traces are qualitatively similar, and have comparable L^2 norms with $\| w^{\text{red}}(.,0) \|_2 = 1.8$ and $\| w^{\text{green}}(.,0) \|_2 = 2.2$. Since $\| f \|_2 = 0.31$, we have $\delta \leq 3.67\text{E-}6$, and $\delta/M \leq 1.67\text{E-}6$. Evidently, the two valid distinct solutions, $w^{\text{green}}(x,1)$ and $w^{\text{red}}(x,1)$, are extremely close to each other. Significantly more accurate data $f(x)$ might be needed to reconstruct the correct initial value $w_0^{\text{red}}(x)$. Such accuracy is highly unlikely in practice. This is in sharp contrast to Figure 3, where, with a 400 times larger L^∞ residual of 3.1E-3, the reconstructions $w_0^{\text{red}}(x)$ and $w_0^{\text{green}}(x)$ are reasonably comparable. Clearly, accurate backward recovery may be intractable in some nonlinear parabolic equations. This is a reflection of ill behavior in the Hölder exponent $\mu(t)$, as illustrated in Figure 1.

7. Example 3 (Figure 4). Linear non-self-adjoint

Effective non-uniqueness is easily achieved in non-self-adjoint problems. With $a = 0.05, \alpha = 0.25, \sigma = 0.125$, consider

$$\begin{aligned} w_t &= a\left\{e^{(\sigma x+\alpha t)}w_x\right\}_x + 0.25w_x, \quad -1 < x < 1, \;\; 0 < t \leq 1.0, \\ w(x,0) &= e^{2x}\sin^2(3\pi x), \quad -1 \leq x \leq 1, \quad w(-1,t) = w(1,t) = 0, \;\; t \geq 0. \end{aligned} \tag{18}$$

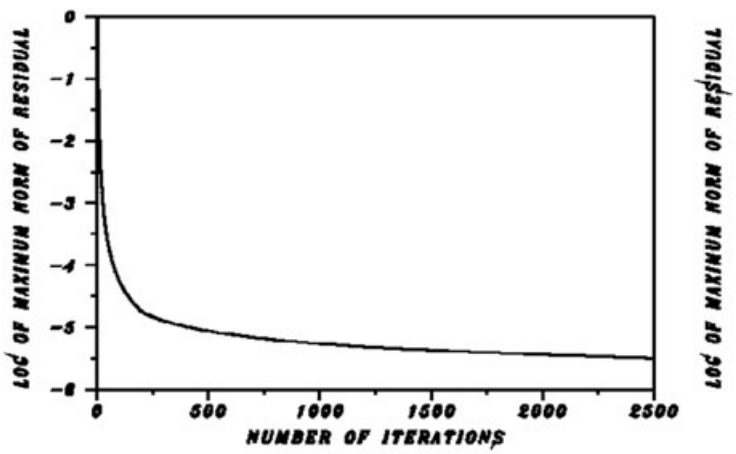

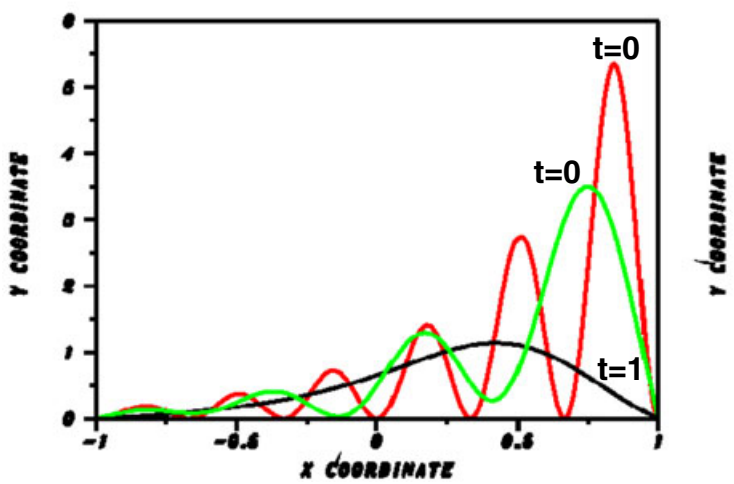

Figure 4. Top. Behavior of $log\{\| f - S[h^n] \|_\infty\}$ for the first 2500 iterations n, in Van Cittert procedure in Example 3. Bottom. Ill behavior in non-self-adjoint problem. Data $f(x)$ (black curve), approximating solution $w^{\text{red}}(x,t)$ at time $t = 1$ with an L^2 relative error of 0.03%, recovers strikingly different initial value $w_0^{\text{green}}(x)$, in lieu of true initial value $w_0^{\text{red}}(x)$.

The initial value $w_0^{\text{red}}(x)$ in (18) is shown as the red trace in Figure 4 (bottom), while the computed approximation $f(x)$ to $w^{\text{red}}(x,1)$ is shown as the black trace in the same figure. By using $f(x)$ in (14), the Van Cittert procedure was applied for 2500 iterations and resulted in $h^{2500}(x) = w_0^{\text{green}}(x)$, shown as the green trace in Figure 4 (bottom), with a final L^∞ residual of 3.6E-4, and an L^2 relative error at $t = 1$ of 0.03%. That relative error is 10 times smaller than was the case in the self-adjoint problem in Example 1. The behavior of $\log\{\| f - S[h^n] \|_\infty\}$ versus n is shown in Figure 4 (top). Here, $\| w_0^{\text{red}} \|_2 = 1.55$, while $\| w_0^{\text{green}} \|_2 = 1.31$. Therefore, both solutions $w^{\text{red}}(x,t)$ and $w^{\text{green}}(x,t)$ in Example 3 satisfy

$$\| w(.,1) - f \|_2 \leq \delta \leq 0.0003 \| f \|_2, \quad \| w(.,0) \|_2 \leq M = 1.6. \tag{19}$$

Since $\| f \|_2 = 0.635$, we have $\delta \leq$ 1.9E-4, and $\delta/M \leq$ 1.23E-4. Again, even though it is substantially different from $w_0^{\text{red}}(x)$, $w_0^{\text{green}}(x)$ must be considered a valid reconstruction of the initial data corresponding to the given data $f(x)$ at $t = 1$. Evidently, such data closely approximate at least two very distinct solutions of the parabolic problem in (18). Significantly, both solutions $w^{\text{red}}(x,t)$ and $w^{\text{green}}(x,t)$ are non-negative on $-1 \leq x \leq 1$, $0 \leq t \leq 1$, and $w_0^{\text{green}}(x)$ is less oscillatory than is $w_0^{\text{red}}(x)$. Non-negativity and smoothness constraints are often applied to regularize ill-posed inverse problems. However, imposing smoothness and non-negativity constraints in this example would clearly not prevent the 'false' solution $w^{\text{green}}(x,t)$. Moreover, there is no obvious qualitative behavior in $w_0^{\text{green}}(x)$ that would arouse suspicion.

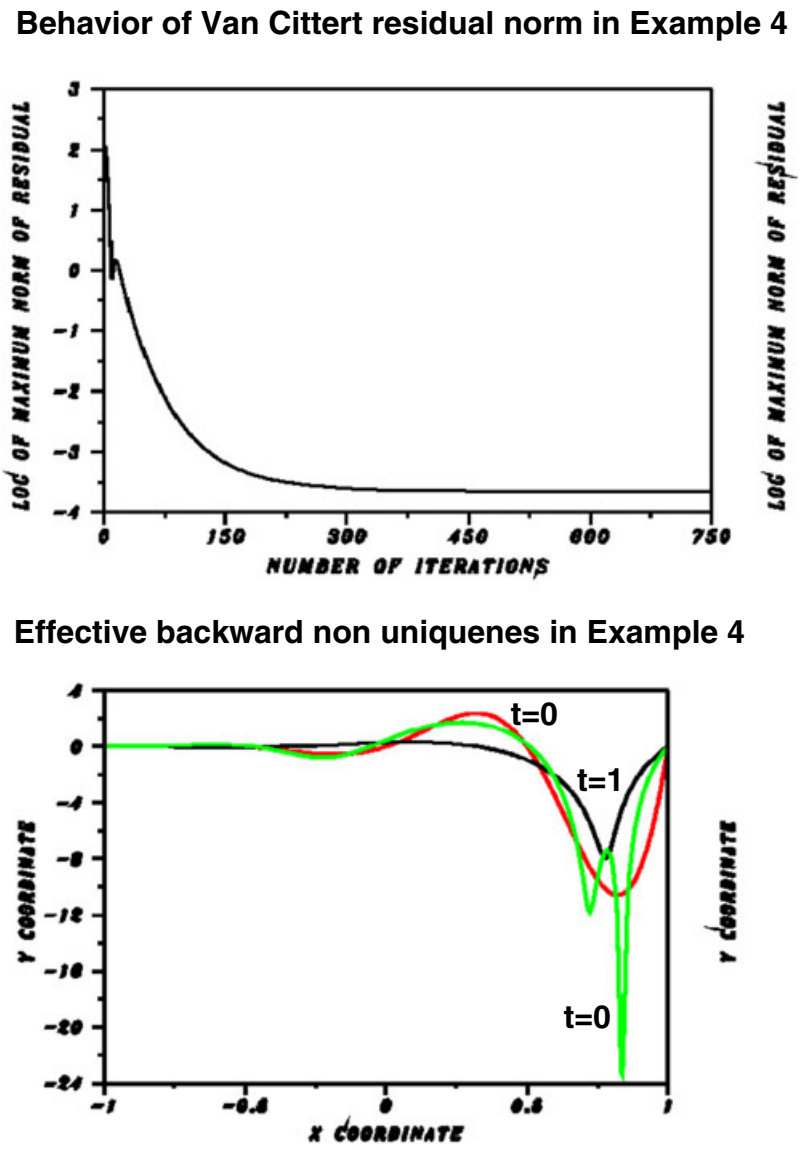

Figure 5. Top. Behavior of $log\{\| f - S[h^n] \|_\infty\}$ for first 750 iterations n, in Van Cittert procedure in Example 4. Bottom. Ill behavior in strongly nonlinear problem. Data $f(x)$ (black curve), approximating solution $w^{\text{red}}(x,t)$ at time $t = 1$ with an L^2 relative error of 0.38%, recovers substantially different initial value $w_0^{\text{green}}(x)$, in lieu of true initial value $w_0^{\text{red}}(x)$.

Published 2012. This article is a US Government work and is in the public domain in the USA.

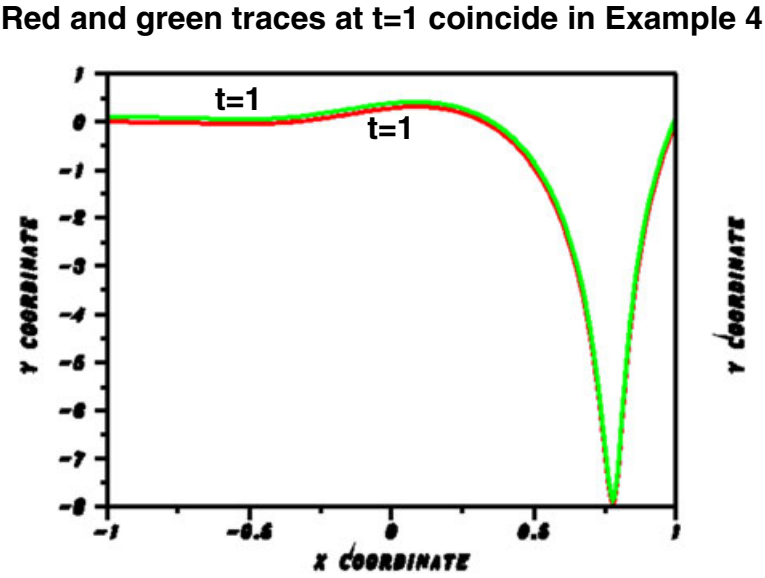

Figure 6. Red and green traces are the solutions at time $t = 1$, $w^{\text{red}}(x,1)$, $w^{\text{green}}(x,1)$, corresponding to the initial values $w_0^{\text{red}}(x)$, $w_0^{\text{green}}(x)$, in Figure 5 (bottom). Traces at $t = 1$ agree to within $2.6E-2$, pointwise. Similar close visual agreement occurs in all previous examples, illustrating the difficulty of recovering $w_0^{\text{red}}(x)$ from approximate values for $w^{\text{red}}(x,1)$.

If the perturbed approximation $f^{\dagger}(x) = f(x)\left\{1.0 + 0.035\cos\left(e^{f(x)}\right)\right\}$, is used in the Van Cittert procedure (14) in lieu of $f(x)$, a different initial value $w_0^{\text{blue}}(x)$ results after 2500 iterations, with a larger L^{∞} residual of 3.98E-2 and a larger L^2 relative error of 2.96% at $t = 1$. However, this well-behaved candidate (not shown) now has oscillatory behavior with both positive and negative values.

8. Example 4 (Figures 5 and 6). Strongly nonlinear

We now consider parabolic equations where the diffusion coefficient is a nonlinear function of the solution,

$$\begin{aligned} w_t &= 0.05\left(e^{0.4w}w_x\right)_x, \quad -1 < x < 1, \ \ 0 < t \le 1.0, \\ w(x,0) &= e^{3x}\sin(2\pi x), \quad -1 \le x \le 1, \ \ w(-1,t) = w(1,t) = 0, \ \ t \ge 0. \end{aligned} \tag{20}$$

The initial value $w_0^{\text{red}}(x)$ in (20) is shown as the red trace in Figure 5 (bottom), while the computed approximation $f(x)$ to $w^{\text{red}}(x,1)$ is shown as the black trace in the same figure. By using $f(x)$ in (14), the Van Cittert procedure was applied for 750 iterations, resulting in a final L^{∞} residual of 2.6E-2 and an L^2 relative error of 0.38% at $t = 1$. That relative error is about the same as was the case in Example 1. The function $h^{750}(x) = w_0^{\text{green}}(x)$ is the green trace in Figure 5 (bottom). The behavior of $\log\{\| f - S[h^n] \|_{\infty}\}$ versus n is shown in Figure 5 (top). Here, $\| w_0^{\text{red}} \|_2 = 3.7$, while $\| w_0^{\text{green}} \|_2 = 3.9$. Therefore, both solutions $w^{\text{red}}(x,t)$ and $w^{\text{green}}(x,t)$ in Example 4 satisfy

$$\| w(.,1) - f \|_2 \le \delta \le 0.0038 \| f \|_2, \qquad \| w(.,0) \|_2 \le M = 3.9. \tag{21}$$

Since $\| f \|_2 = 1.95$, we have $\delta \le 7.4E\text{-}3$, and $\delta/M \le 1.9E\text{-}3$. The traces for $w^{\text{red}}(x,1)$ and $w^{\text{green}}(x,1)$ are plotted in Figure 6 and are visually indistinguishable. The green trace in Figure 6 was artificially raised by a small amount, so as to render the red trace visible. Evidently, $w_0^{\text{green}}(x)$ is a valid reconstruction. Note, however, that $\| w_0^{\text{red}} \|_{\infty} = 10.6$, while $\| w_0^{\text{green}} \|_{\infty} = 23.4$ is more than twice as large. Accurate prior knowledge of the L^{∞} norm of $w(x,0)$ in (20), *if available*, might be used to reject $w_0^{\text{green}}(x)$ as false.

9. Example 5 (Figures 7 and 8). Strongly nonlinear

While the level of accuracy in this final example is lower than in the preceding examples, that accuracy is representative of several practical applications. Consider the nonlinear problem with non-negative solution

$$\begin{aligned} w_t &= 0.05\left(e^{0.5w}w_x\right)_x + ww_x, \quad -1 < x < 1, \ \ 0 < t \le 1.0, \\ w(x,0) &= e^{3x}\sin^2(3\pi x), \quad -1 < x < 1, \ \ w(-1,t) = w(1,t) = 0, \ \ t > 0. \end{aligned} \tag{22}$$

The initial value $w_0^{\text{red}}(x)$ in (22) is shown as the red trace in Figure 7 (bottom), while the computed approximation $f(x)$ to $w^{\text{red}}(x,1)$ is shown as the black trace in the same figure. Here, $\| f \|_2 = 1.15$, and $\| w_0^{\text{red}} \|_2 = M = 3.3$. By using $f(x)$ in (14), behavior in the Van Cittert

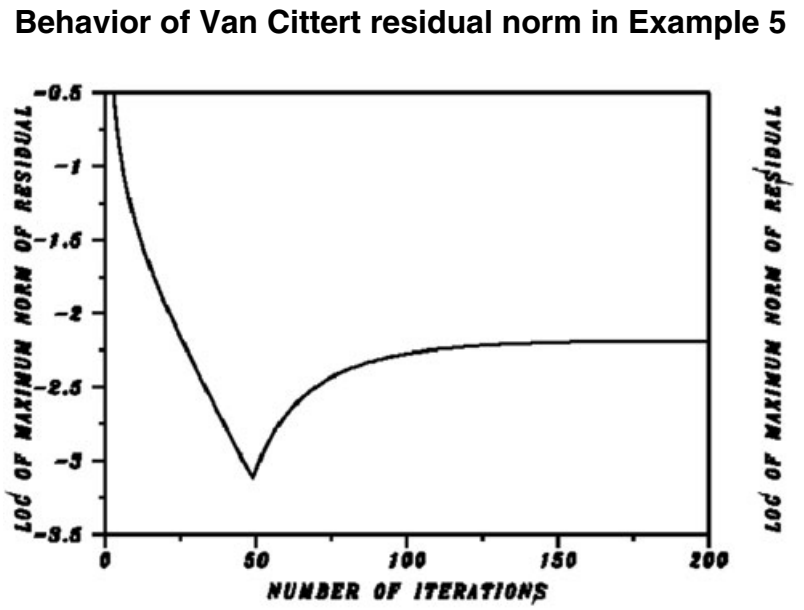

Figure 7. Top. Behavior of $log\{\| f - S[h^n] \|_\infty\}$ for first 200 iterations n, in Van Cittert procedure in Example 5. Bottom. Use of realistic levels of accuracy in strongly nonlinear problem. Data $f(x)$ (black curve) approximating solution $w^{\text{red}}(x,t)$ at time $t = 1$ with an L^2 relative error of 3.24% recover quite plausible, but vastly different initial values $w_0^{\text{blue}}(x)$, $w_0^{\text{green}}(x)$, in lieu of true initial value $w_0^{\text{red}}(x)$. Subsequent evolutions of $w_0^{\text{green}}(x)$ and $w_0^{\text{red}}(x)$ are shown in Figure 8.

iteration is shown in Figure 7 (top). The L^∞ residual after 50 iterations has the value 4.7E-2, and the function $h^{50}(x) = w_0^{\text{green}}(x)$ is the green trace in Figure 7 (bottom). The L^2 relative error at $t = 1$, $\| f - S[h^{50}] \|_2 / \| f \|_2 =$ 2.68%. Next, if we perturb $f(x)$ to form $f^\dagger(x) = f(x)\left\{1.0 + 0.025\cos\left(e^{f(x)}\right)\right\}$ and use $f^\dagger(x)$ in the Van Cittert iteration, we obtain $h^{47}(x) = w_0^{\text{blue}}(x)$, the blue trace in Figure 7 (bottom), with a slighly larger L^∞ residual of 5.4E-2, as well as a slightly larger L^2 relative error of 3.24% at $t = 1$. Thus, $\delta \leq$ 3.7E-2, and $\delta/M \leq$ 1.2E-2. We stress that while these errors are larger than was the case in the well-behaved self-adjoint problem in Example 1, such errors would not be considered unreasonable in many engineering contexts involving real data. Indeed, the red, green, and blue traces in this example demonstrate the *existence* of at least three very distinct initial values at $t = 0$ that would be compatible with the data at $t = 1$, at common levels of data uncertainty. In Figure 8, it is instructive to compare the time evolution of $w_0^{\text{green}}(x)$ into $f(x)$ at $t = 1$, with the corresponding evolution of $w_0^{\text{red}}(x)$. The evolution of $w_0^{\text{green}}(x)$ is simple, easily understood, and plausible. The evolution of $w_0^{\text{red}}(x)$ is quite complex and not as easily anticipated. As was the case in Example 3, imposing smoothness and non-negativity constraints in

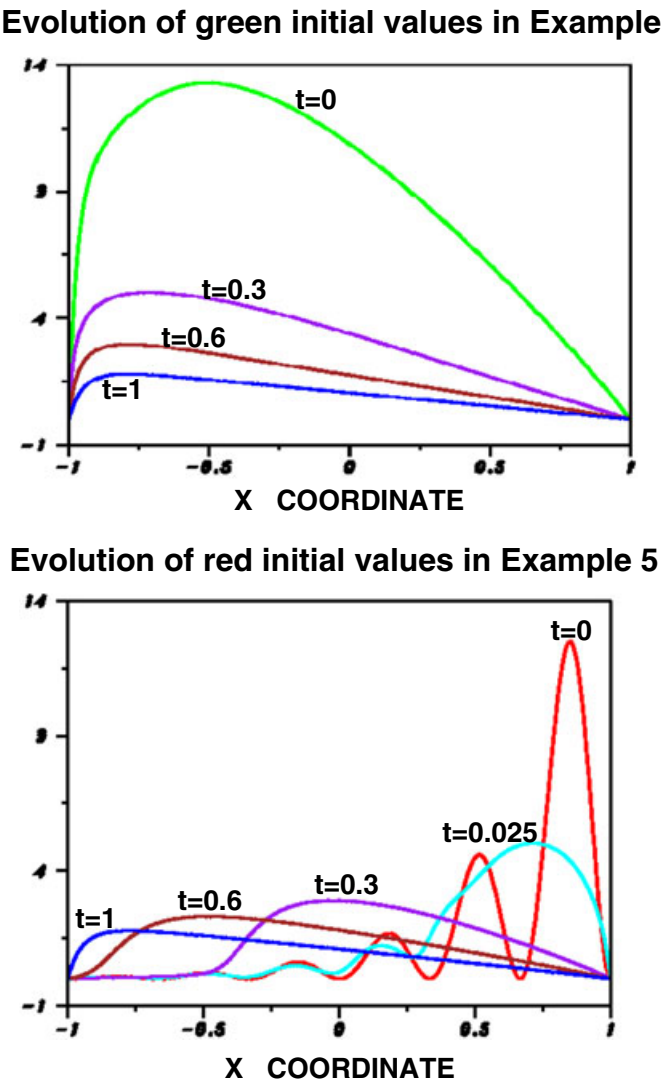

Figure 8. Comparing the time evolutions of $w_0^{\text{green}}(x)$ and $w_0^{\text{red}}(x)$ as t increases from $t = 0$ to $t = 1$ in Example 5. The evolution of $w_0^{\text{green}}(x)$ into $f(x)$ at $t = 1$, is simple and quite plausible, while the corresponding evolution of $w_0^{\text{red}}(x)$ is quite complex and not as easily anticipated.

Example 5 would not eliminate the candidates $w_0^{\text{green}}(x), w_0^{\text{blue}}(x)$. In Example 4, accurate prior knowledge of the L^∞ norm at $t = 0$, rather than the L^2 norm, could be used to reject $w_0^{\text{green}}(x)$. In the present case, all three candidates have comparable L^∞ norms, with $\| w_0^{\text{red}} \|_\infty = 13.3$, $\| w_0^{\text{green}} \|_\infty = 12.5$, and $\| w_0^{\text{blue}} \|_\infty = 16.0$. However, $\| w_0^{\text{red}} \|_2 = 3.3$, while $\| w_0^{\text{green}} \|_2 = 9.7$, and $\| w_0^{\text{blue}} \|_2 = 9.9$. The fact that $w_0^{\text{blue}}(x)$ and $w_0^{\text{green}}(x)$ have comparable L^2 norms, together with the plausible simple evolution of $w_0^{\text{green}}(x)$ into $f(x)$ in Figure 8, might lead to possible rejection of the true solution $w_0^{\text{red}}(x)$, given its complex evolution and substantially smaller L^2 norm. In contrast to Example 4, accurate prior knowledge of the L^2 norm at $t = 0$, rather than the L^∞ norm, would be beneficial in this example.

10. Concluding remarks

In recent years, there has been considerable interest in the numerical computation of ill-posed inverse problems, as a result of growth in such fields as nondestructive evaluation, geophysical prospecting, remote sensing, diagnostic imaging in medical and industrial applications, and other related areas. One central question, that of stabilizing ill-posed computations so as to prevent explosive noise amplification, has received much attention. This is the regularization problem, which has spawned a large literature.

The problem discussed in this paper is unrelated to such noise amplification, but is equally serious. While backward uniqueness of solutions holds true for large classes of linear and nonlinear parabolic equations, the exact, highly restricted data at time $t = 1$ necessary to recover a particular solution, is seldom available. One must rely on approximate data. However, such data may unexpectedly approximate several distinct plausible solutions at time $t = 1$.

Published 2012. This article is a US Government work and is in the public domain in the USA.

Math. Meth. Appl. Sci. ***2013***, 36 249–261

This paper has focused attention on a class of 1D parabolic equations $w_t = Lw$ and presented several examples where there is strong computational evidence for the existence of distinct solutions $w^{\text{red}}(x,t)$ and $w^{\text{green}}(x,t)$ on $0 \le t \le 1$, having the following properties:

- The quantity $\| w^{\text{red}}(.,1) - w^{\text{green}}(.,1) \|_\infty$ is small enough that the traces $w^{\text{red}}(x,1)$ and $w^{\text{green}}(x,1)$ at $t = 1$ are visually indistinguishable when plotted.
- The L^2 relative error at $t = 1, \{\| w^{\text{red}}(.,1) - w^{\text{green}}(.,1) \|_2 / \| w^{\text{red}}(.,1) \|_2\}$ is generally less than 1%.
- The functions $w^{\text{red}}(x,0)$ and $w^{\text{green}}(x,0)$ are smooth, well-behaved, physically plausible, and entirely different. Except in the case of Example 5, these functions have comparable L^2 norms.

In these examples, there is effective non-uniqueness in the recovery of $w^{\text{red}}(x,0)$ in the stabilized backward problem (4), (5), because reasonably accurate data $f(x)$ for the unknown $w^{\text{red}}(x,1)$ also approximates $w^{\text{green}}(x,1)$. As noted in Section 1, a large variety of numerical methods for backward parabolic equations exists. The present results raise fundamental questions regarding the general reliability of solutions computed with any such method. Given reasonably accurate data $f(x)$ at time $t = 1$, the physically meaningful, highly plausible, solution $w^{\text{green}}(x,t)$ obtained with that method, may be vastly different from the true solution $w^{\text{red}}(x,t)$ in the actual engineering situation at hand. Moreover, there may be no indication that $w^{\text{green}}(x,t)$ is a false solution, and traditional smoothness and positivity constraints may not prevent the occurrence of such spurious solutions.

The Van Cittert iterative procedure was a vital part of this investigation. While that iteration seldom converges and can behave unpredictably and even diverge in some cases, it is able to generate unexpected, valid, noise free, candidate solutions $w^{\text{green}}(x,t)$. Small perturbations of the data $f(x)$ input into the Van Cittert procedure can produce additional candidates $w^{\text{blue}}(x,t)$, as noted in Examples 3 and 5. Other iterative procedures might be found that produce further viable, yet distinctly different, initial functions $w(x,0)$ from the same data $f(x)$. Such multiple possible solutions explain why the inequality (13) does not guarantee any accuracy at $t = 0$, but only provides the redundant information $\| w^1(.,0) - w^2(.,0) \|_2 \le 2M$.

The Hölder exponent $\mu(t)$ in the inequality (13) plays an important behind the scenes role in the above examples. That exponent is a property of the particular parabolic equation, and it reflects how fast that equation forgets the past. It may be viewed as a barometer on the difficulty of backward reconstruction. The relatively well-behaved self-adjoint problem in Example 1, corresponds to the best possible case where $\mu(t) = t$. However, as shown in [32] and illustrated in Figure 1, non-self-adjointness, nonlinearity, and other adverse properties of the elliptic spatial operator L in (4) can cause significantly faster decay of $\mu(t)$ to zero, as $t \downarrow 0$. The intractable recovery of $w_0^{\text{red}}(x)$ in the Burgers equation in Example 2 is especially noteworthy.

These unexpected results imply a need for caution in applying backward parabolic equations. There is ever growing interest in the use of backward parabolic equations as an all-purpose image sharpening tool. Images blurred by space variant, non-isotropic, Gaussian-like point spread functions, are equivalent to solutions of 2D linear non-self-adjoint parabolic equations, with variable coefficients. Example 3 suggests that false deblurred images are possible from approximately known blurred image data, even with very little noise. Likewise, in the 2D or 3D advection dispersion equation (1), plausible, yet false, backward solutions are possible from an approximately known contaminant spatial distribution at the current time T.

References

1. Han H, Ingham DB, Yuan Y. The boundary element method for the solution of the backward heat conduction equation. *Journal of Computational Physics* 1995; **116**:292–299.
2. Ames KA, Epperson JF. A kernel-based method for the approximate solutions of backward parabolic problems. *SIAM Journal on Numerical Analysis* 1997; **34**:1357–1390.
3. Buzbee BL, Carasso AS. On the numerical computation of parabolic problems for preceding times. *Mathematics of Computation* 1973; **27**:237–266.
4. Cannon JR. Some numerical results for the solution of the heat equation backwards in time. In *Proc. Adv. Sympos. Numerical Solutions of Nonlinear Diffferential Equations (Madison, WI 1966)*. Wiley: New York, 1966; 21–54.
5. Ewing RE. The approximation of certain parabolic equations backward in time by Sobolev equations. *SIAM Journal on Mathematical Analysis* 1975; **6**:283–294.
6. Hào DN, Duc NV, Lesnic D. Regularization of parabolic equations backward in time by a non-local boundary value method. *IMA Journal of Applied Mathematics* 2010; **75**:291–315.
7. Höhn W. Finite elements for parabolic equations backwards in time. *Numerische Mathematik* 1982; **40**:207–227.
8. Johansson BT, Lesnic D, Reeve T. A comparative study on applying the method of fundamental solutions to the backward heat conduction problem. *Mathematical and Computer Modelling* 2011; **54**:403–416.
9. Lattès R, Lions JL. *The Method of Quasi-reversibility*. American Elsevier: New York, 1969.
10. Lee J, Sheen D. A parallel method for backward parabolic problems based on the Laplace transformation. *SIAM Journal on Numerical Analysis* 2006; **44**:1466–1486.
11. Lesnic D, Elliott L, Ingham DB. An iterative boundary element method for solving the backward heat conduction equation using an elliptic approximation. *Inverse Problems in Engineering* 1998; **6**:255–279.
12. Liu C-S. An efficient backward group preserving scheme for the backward in time Burgers equation. *Computer Modeling in Engineering and Sciences* 2006; **12**:55–65.
13. Marbán JM, Palencia C. A new numerical method for backward parabolic problems in the maximum-norm setting. *SIAM Journal on Numerical Analysis* 2002; **40**:1405–1420.
14. Mera NS, Elliott L, Ingham DB, Lesnic D. An iterative boundary element method for solving the one-dimensional backward heat conduction problem. *International Journal of Heat and Mass Transfer* 2001; **44**:1937–1946.
15. Tuan NH, Trong DD. A nonlinear parabolic equation backward in time: regularization with new error estimates. *Nonlinear Analysis: Theory, Methods and Applications* 2010; **73**:1842–1852. DOI: 10.1016/j.na.2010.05.019.

16. Atmadja J. The marching-jury backward beam equation method and its application to backtracking non-reactive plumes in groundwater. *PhD Dissertation*, Columbia University, 2001.
17. Atmadja J, Bagtzoglou AC. Pollution source identification in heterogeneous porous media. *Water Resources Research* 2001; **37**:2113–2125. DOI: 10.1029/2001WR000223.
18. Bagtzoglou AC, Atmadja J. Marching-jury backward beam equation and quasi-reversibility methods for hydrologic inversion: application to contaminant plume spatial distribution recovery. *Water Resources Research* 2003; **39**:1038–1052. DOI: 10.1029/2001WR001021.
19. Bagtzoglou AC, Atmadja J. Mathematical methods for hydrologic inversion: the case of pollution source identification. *Handbook of Environmental Chemistry, Water Pollution Series* Vol. 5, Part F, 2005:65–96.
20. Baun SA, Bagtzoglou AC. A computationally attractive approach for near real-time contamination source identification. *Developments in Water Science* 2004; **55**:1263–1271. DOI: 10.1016/S0167-5648(04)80141-2.
21. Liu C-S, Chang C-W, Chang J-R. The backward group preserving scheme for 1D backward in time advection–dispersion equation. *Numerical Methods for Partial Differential Equations* 2008; **26**:61–80.
22. Neupauer RM, Wilson JL. Backward probabilistic model of groundwater contamination in non-uniform and transient flow. *Advances in Water Resources* 2002; **25**:733–746.
23. Skaggs TH, Kabala ZJ. Recovering the history of a groundwater contaminant plume: method of quasi-reversibility. *Water Resources Research* 1995; **31**:2669–2673. DOI: 10.1029/95WR02383.
24. Carasso AS. Overcoming Hölder continuity in ill-posed continuation problems. *SIAM Journal on Numerical Analysis* 1994; **31**:1535–1557.
25. Carasso AS. Linear and nonlinear image deblurring: a documented study. *SIAM Journal on Numerical Analysis* 1999; **36**:1659–1689.
26. Carasso AS, Sanderson JG, Hyman JM. Digital removal of random media image degradations by solving the diffusion equation backwards in time. *SIAM Journal on Numerical Analysis* 1978; **15**:343–367.
27. Han H, Yan M, Wu C. An energy regularization method for the backward diffusion problem and its applications to image deblurring. *Communications in Computational Physics* 2008; **4**:177–194.
28. Lee J, Sheen D. A parallel method for backward parabolic problems and its application to image deblurring: Part II. Available from: http://www.ksiam.org/conference/annual061/upfile/ksiam_submit_1.pdf, pp. 23–31.
29. Wang L, Luo S, Wang Z. Image deblur with regularized backward heat diffusion. *Image Processing (ICIP), 2010 17th IEEE International Conference Proceedings*, Hong Kong, China, September 26–29 2010; 1141–1144, DOI: 10.1109/ICIP.2010.5651365.
30. Carasso AS. Bochner subordination, logarithmic diffusion equations, and blind deconvolution of Hubble space telescope imagery and other scientific data. *SIAM Journal on Imaging Sciences* 2010; **3**:954–980.
31. Ames KA, Straughan B. *Non-standard and Improperly Posed Problems*. Academic Press: New York, 1997.
32. Carasso AS. Logarithmic convexity and the 'slow evolution' constraint in ill-posed initial value problems. *SIAM Journal on Mathematical Analysis* 1999; **30**:479–496.
33. Knops RJ. Logarithmic convexity and other techniques applied to problems in continuum mechanics. In *Symposium on Non-well-posed Problems and Logarithmic Convexity*, Knops RJ (ed.), Lecture Notes in Math. 316. Springer-Verlag: New York, 1973; 31–54.
34. Knops RJ, Payne LE. On the stability of solutions of the Navier–Stokes equations backward in time. *Archives for Rational Mechanics and Analysis* 1968; **29**:331–335.
35. Payne LE. Improperly posed problems in partial differential equations. In *CBMS-NSF Regional Conference Series in Applied Mathematics*, Vol. 22. SIAM Publications: Philadelphia, PA, 1975.
36. Jansson PA. *Deconvolution with Application in Spectroscopy*. Academic Press: New York, 1984.
37. Lagendijk RL, Biemond J. *Iterative Identification and Restoration of Images*. Kluwer Academic Publishers: Boston, 1991.
38. Berzins M, Dew PM. Algorithm 690: Chebyshev polynomial software for elliptic–parabolic systems of PDEs. *Association of Computing Machinery Transactions on Mathematical Software* 1991; **17**:178–206.